A Compact Optically-Coherent Fiber Frequency Comb

L.C. Sinclair[1], J.-D. Deschênes[1,2], L. Sonderhouse[1], W. C. Swann[1], I.H. Khader[1], E. Baumann[1], N. R. Newbury[1], and I. Coddington[1]

[1]*National Institute of Standards and Technology, 325 Broadway, Boulder, Colorado, 80303, USA*
[2]*Université Laval, Québec City, Québec, Canada*

We describe the design, fabrication, and performance of a self-referenced, optically coherent frequency comb. The system robustness is derived from a combination of an optics package based on polarization-maintaining fiber, saturable absorbers for mode-locking, high signal-to-noise ratio (SNR) detection of the control signals, and digital feedback control for frequency stabilization. The output is phase-coherent over a 1-2 μm octave-spanning spectrum with a pulse repetition rate of ~ 200 MHz and a residual pulse-to-pulse timing jitter < 3 femtoseconds, well within the requirements of most frequency-comb applications. Digital control enables phase coherent operation for over 90 hours, critical for phase-sensitive applications such as timekeeping. We show that this phase-slip free operation follows the fundamental limit set by the SNR of the control signals. Performance metrics from three nearly identical combs are presented. This laptop-sized comb should enable a wide-range of applications beyond the laboratory.

I. INTRODUCTION

Optical frequency combs are powerful instruments which provide millions of mutually-coherent, perfectly-spaced comb modes that are uniquely capable of phase coherently linking the optical, microwave and terahertz regimes. Today's frequency combs support a range of applications and fundamental science[1–4], and frequency combs capable of operation outside of a well-controlled laboratory environment are increasingly necessary as the list of applications grows. This paper describes the design and performance of a fiber-frequency comb, whose development was motivated by needs for improved trace gas measurements[5–16], high-accuracy laser detection and ranging (LADAR)[17–27], and optical free-space time-and-frequency transfer[28] to support future networks of mobile atomic optical clocks.[29–31] These applications and others necessitate the development of a new breed of compact, relatively inexpensive, and environmentally robust frequency combs that can operate outside the laboratory in industrial settings and in moving vehicles, all while maintaining high performance and requiring minimal, or even no, user intervention.

Solid-state combs, micro-resonator-based combs, and fiber-based combs are all potential platforms for development of an environmentally robust comb. Solid-state combs, such as those based on Ti:sapphire, Yb:YAG, or Erbium:Ytterbium-doped glass, now exist with very compact cavities[32–34] and with direct diode pumping.[35] However, solid-state combs require precise free-space alignment, which is challenging and expensive to implement in a robust platform. Recent advances in chip-scale micro-resonator-based combs are intriguing[36–38], but current "micro" combs still significantly lag "macro" combs in performance, overall system size, and robustness, as well as have repetition frequencies of many tens of GHz. Optical-fiber-based frequency combs have long been identified as the best candidate for lower-cost fieldable systems.[39–44] All-fiber designs are impervious to misalignment and can be assembled relatively quickly using common telecommunications fiber handling tools and readily available telecommunications grade micro-optic components. Historically, fiber-based combs have been limited by changes in birefringence in the optical fiber due to strain, temperature changes, or humidity changes. This varying environmentally-induced birefringence results in polarization wander within the fiber. Polarization wander can disrupt mode-locking in several frequency comb designs and can also cause significant spectral drift during supercontinuum generation, impacting both offset-frequency detection and spectral coverage. The advent of high quality polarization-maintaining (PM) fiber and PM fiber-optic components has largely solved this problem.

The strength of fiber-based combs is clear from several demonstrations. A very early design demonstrated turn-key operation through the use of a semiconductor saturable absorbing mirror (SESAM).[41,45] Previously, we demonstrated an optically-coherent frequency comb with a 27 MHz repetition rate that maintained its low-noise performance even when the femtosecond PM-fiber laser was subjected to g-level vibrations.[46] A Korean team launched an all-fiber femtosecond laser with a 25 MHz repetition rate on a satellite, achieving mode-locked operation in low-earth orbit for over a year.[47] A German team has developed a repetition-rate-stabilized PM-fiber frequency comb for planned operation on a sounding rocket.[48] More recently, our group has demonstrated a 200 MHz all-PM fiber frequency comb able to maintain optical coherence both under vibrations of up to 0.5 g rms (integrated from 10 Hz to 1 kHz with a $1/f$ profile) and in a moving vehicle.[49]

In this paper, we present an optical frequency comb design based on Ref. 49 in more detail and modified for improved performance. Compared to the earlier design, the coherence is improved by a factor of two, the output power is 50 % higher, and the overall size of the optics package is reduced by a factor of six to below one liter in volume. In a design compatible with non-laboratory operation, these compact frequency combs achieve a residual pulse-to-pulse timing jitter of < 3 femtoseconds and residual sub-radian optical coherence at the comb center wavelength. Additionally, we have demonstrated phase-slip-free operation for over 90 hours driven by the combination of high signal-to-noise-ratio (SNR) phase-locking signals and digitally-based phase detection and feedback. This level of performance exceeds that required to support demanding applications, such as high resolution frequency-comb spectroscopy, optical time-frequency transfer, and precision LADAR.[13,16,25,28] The layout of this paper is as follows: Section II describes the optical design and fabrication procedure for the frequency comb. Section III describes the feedback actuators and phase locking electronics used to achieve an optically coherent, self-referenced comb. Section IV discusses the performance of the frequency comb in terms of phase noise, optical coherence, and "phase-slip" free operation. As discussed in Section IV, all of the performance metrics represent residual, in-loop values, i.e. these represent the limit of comb performance in the absence of an absolute optical reference. Appendices A through C address the fiber lengths and types, a method to build a comb with a specific repetition rate, and packaging of the optical system.

II. FREQUENCY COMB OPTICAL SYSTEM

The design presented here is based on three similar frequency combs that have been operating continuously in our lab for durations up to a year. These combs, hereafter labelled "A", "B" and "C", operate with a pulse repetition-rate (comb mode spacing) near 200 MHz, but more recent versions operate equally well at repetition rates from 100 to 300 MHz with only modest changes to the amplifier.

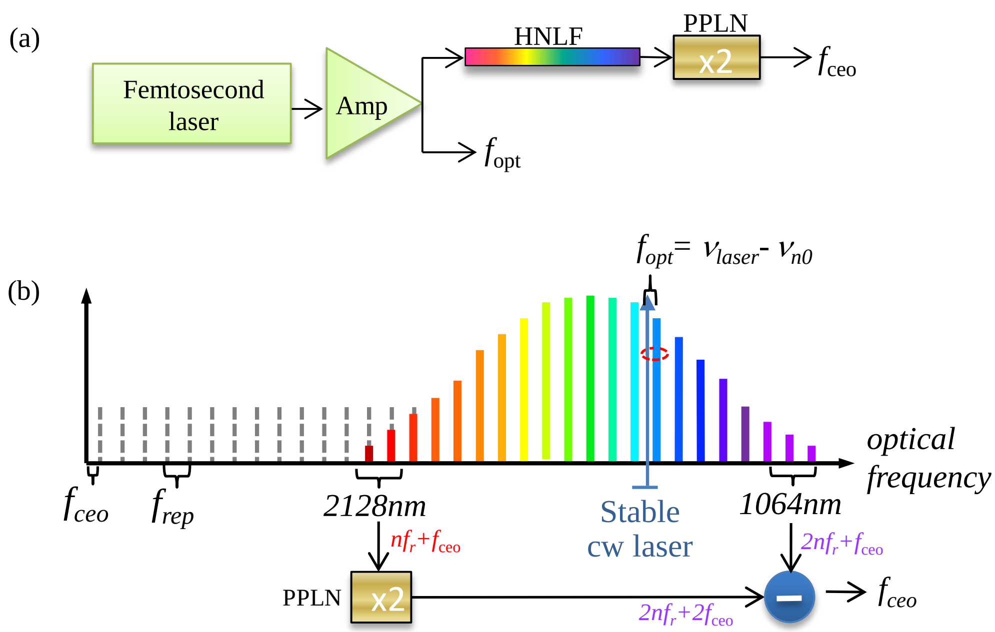

FIG. 1 (a) Generalized schematic of a fiber frequency comb. The heart of a frequency comb is the mode-locked femtosecond laser, which produces a spectrum of discrete comb modes spaced by the repetition frequency, f_{rep}, covering a modest spectral bandwidth. This initial comb structure is amplified and further spectrally broadened to an octave in highly nonlinear fiber (HNLF) to produce the spectrum idealized in part (b). Periodically poled lithium niobate (PPLN) is used to compare the two ends of this optical spectrum for stabilization of the carrier-envelope-offset frequency, f_{ceo}. (b) Idealized frequency comb showing relevant optical and RF frequencies. The frequency of the n^{th} comb mode is given by the standard comb equation $\nu_n = nf_{rep} + f_{ceo}$. The comb is stabilized by phase-locking the RF heterodyne frequency, f_{opt}, between the n_0^{th} comb mode of frequency, ν_0, and a stable cw laser of frequency, ν_{laser}, and by phase-locking the RF carrier-envelope-offset frequency f_{ceo}, which is generated via the conventional $1f$-to-$2f$ detection scheme.[50]

The basic concept of the frequency comb is reviewed in Fig. 1.[1,2] While "free-running combs" – i.e. unstabilized mode-locked lasers – are adequate for some applications, our interest here is in a fully stabilized, or phase-locked, frequency comb. For a fully-stabilized frequency comb, all comb modes are simultaneously stabilized by the stabilization of only two degrees of freedom. Here, the two degrees of freedom are the carrier-envelope-offset frequency, f_{ceo}, and a single optical comb mode whose frequency is near to an optical standard, i.e. cavity-stabilized laser (or future optical clock transition), as illustrated in Fig. 1b. This optical stabilization provides phase coherence across the optical spectrum, greatly increasing the comb performance and range of possible applications compared to the alternative direct stabilization of the repetition rate.[50] A detailed discussion of comb stabilization is provided in Section III.

A. Polarization-Maintaining Fiber Design

The fiber frequency comb design consists solely of PM single-mode fiber. Six different types of PM fibers are used. (See Appendix A.) All six have Panda-type stress rods to provide the difference in index between the fast and slow axes; other PM-fiber types with similar properties could be substituted. The gain medium for both the femtosecond fiber-laser and the fiber amplifier is provided by Erbium (Er) doped fibers. A PM highly nonlinear fiber (HNLF) enables generation of the octave-spanning spectrum.[51] In addition, standard telecommunications Panda PM-980 and PM-1550 fibers are used. The all-PM-fiber design requires a PM fiber fusion-splicer for comb fabrication and typical splice losses for the frequency comb optical system are < 0.5 dB.

B. The Femtosecond Laser Cavity

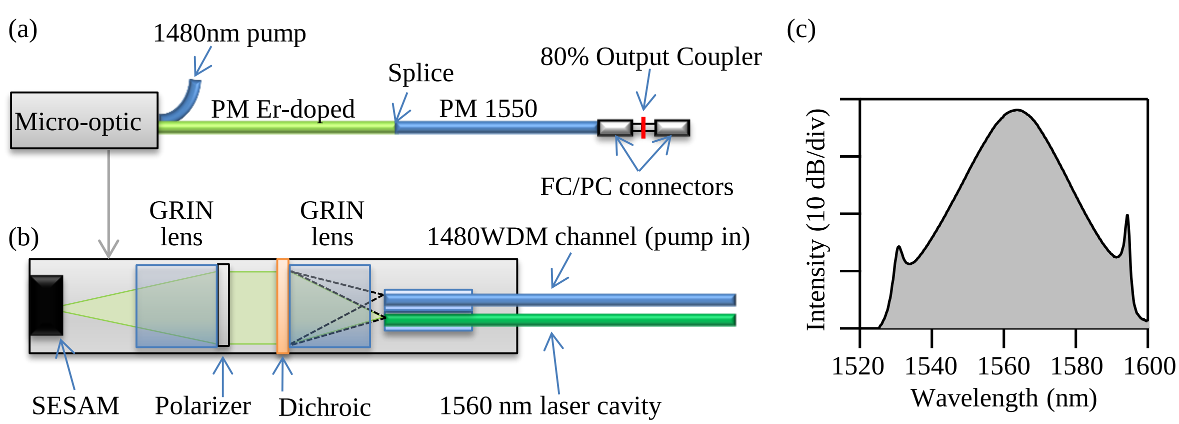

FIG. 2. (a) The femtosecond laser consists of the linear cavity bounded by the semiconductor saturable absorbing mirror (SESAM) on one end and the 80 % reflective dielectric coated output coupler on the other end. (b) Micro-optic design. (c) Output spectrum with a full-width-half-max (FWHM) of 12.2 nm.

At the heart of the frequency comb system is an all-PM-fiber femtosecond laser cavity. As a positive feedback system, the femtosecond laser is generally the most delicate part of any frequency comb and must generate an uninterrupted, optically coherent, low timing-jitter train of pulses that will propagate through the rest of the system. Therefore, we have selected a simple femtosecond laser design, offloading as much of the power and optical-bandwidth generation as possible onto the amplifier.

Figure 2 shows the simple linear all-PM-fiber cavity, consisting of PM Er-doped fiber spliced to a PM-1550 fiber. The output coupler is formed by a FC/PC connector junction where the face of one FC/PC connector has been coated with an 80% reflective dielectric coating. The output coupler is discussed in detail in Appendix B. At the other end of the cavity, the PM Er-doped fiber is coupled into a custom micro-optic component containing a SESAM to enable self-starting mode-locked operation.[23,34,41,45,52] The Er-doped fiber length is not critical and ranges from 8.5 cm to 16.5 cm (see Table II in Appendix A); however, the shorter length of 8.5 cm is close to the minimal length for laser operation. Lengths longer than 16.5 cm tend to shift the laser spectrum to longer wavelengths making later amplification and compression stages more difficult. The PM-1550 fiber forms the remainder of the cavity and has the requisite length (of ~ 33.5 to 41.5 cm) to support a repetition rate of 200 MHz. Appendix B discusses a method to achieve an exact repetition rate, which is critical in applications such as dual-comb spectroscopy[53] or microwave generation through optical frequency division.[54] The femtosecond laser achieves self-starting mode-locked operation with an output of 10 mW and a 12 – 13 nm spectral bandwidth centered around 1560 nm (see Fig. 2c) and pulse widths of 200 - 220 fs for combs A - C.

Manufacturing of the custom micro-optic component is well within the capabilities of fiber component suppliers and serves several critical functions. First, the spot-size on the SESAM must be tuned to achieve a fluence of approximately twice the SESAM saturation value to optimize the femtosecond laser spectral bandwidth and pulse duration. The use of a gradient index (GRIN) lens inside the micro-optic housing (Fig. 2b) expands the beam to a 20 μm diameter spot size, twice the diameter that would result from directly butt-coupling the fiber to the SESAM. Given our ~50 mW intracavity power, the pulse intensity at the SESAM is twice the SESAM saturation intensity of 50 $\mu J/cm^2$. The SESAM used here has a 2 ps relaxation time constant, 6% modulation depth and a 9% low signal absorption. The lens-based design also reduces the risk of damage to the SESAM.[55] The micro-optic contains two other critical components. First, it contains a polarizer aligned with the slow-axis of the PM fiber, which then defines the polarization of the femtosecond laser. Second, it contains a dichroic mirror to allow for the injection of the 1480-nm light that pumps the Er-doped gain fiber. In our original design of Ref 49, the laser was pumped at 980 nm. However, 1480-nm pump light is preferred for the following reason: The frequency comb noise is driven by the pump-laser relative-intensity-noise (RIN). This RIN is minimized by: (i) inserting an isolator between the pump diode and the femtosecond laser cavity, and (ii) operating the pump diode at maximum power followed by an attenuator to reach the desired pump power for the femtosecond laser. (This is done to take advantage of the fact that the pump RIN increases as the square root of its power – running the pump at its maximum power and attenuating to the power desired by the laser effectively results in a lower pump RIN seen by the laser.) Both isolators and attenuators are lower cost, more compact, and more efficient at 1480 nm than at 980 nm.

Both the Er-doped fiber and the PM-1550 fiber in the cavity are anomalous dispersion fiber, yielding a net round-trip dispersion of -0.22 ps^2, leading to soliton mode-locking. This intra-cavity dispersion is high compared to other designs[44,56–58], which increases the carrier-envelope-offset noise.[44,57,59] However, this high dispersion offers several advantages. First, small changes in the net dispersion due to fiber length variations have little overall impact on the femtosecond laser performance leading to a more reproducible design. Second, both the PM Er-doped and PM-1550 fibers have a similar dispersion of ~17 ps/nm/km at 1550 nm, so modest variations in their relative lengths have nearly inconsequential impact on laser performance. Finally, recent theoretical studies have shown that a soliton-wake instability[60] is possible for low dispersion cavities if the SESAM time constant is too long. This soliton-wake instability interferes with mode-locking of the laser. At the relatively high net dispersion here for the 2 ps SESAM time constant, the mode-locking is robust. At lower anomalous dispersions of 0 to -0.1 ps^2 mode-locking is not observed presumably due to this instability.

C. Amplification and Spectral Broadening

The femtosecond laser is followed by an amplifier, an HNLF for spectral broadening, and a periodically-poled lithium niobate (PPLN) waveguide to double the wavelengths near 2 μm for the 1f-to-2f method of detection of f_{ceo}. The full fiber design is considerably more complicated than Fig. 1a and is given in Figure 3. While the fiber and fiber-optic components occupy less than 0.1 L in volume, they are enclosed in 0.7 L package (Appendix C). Appendix A provides detailed information on fiber types and lengths.

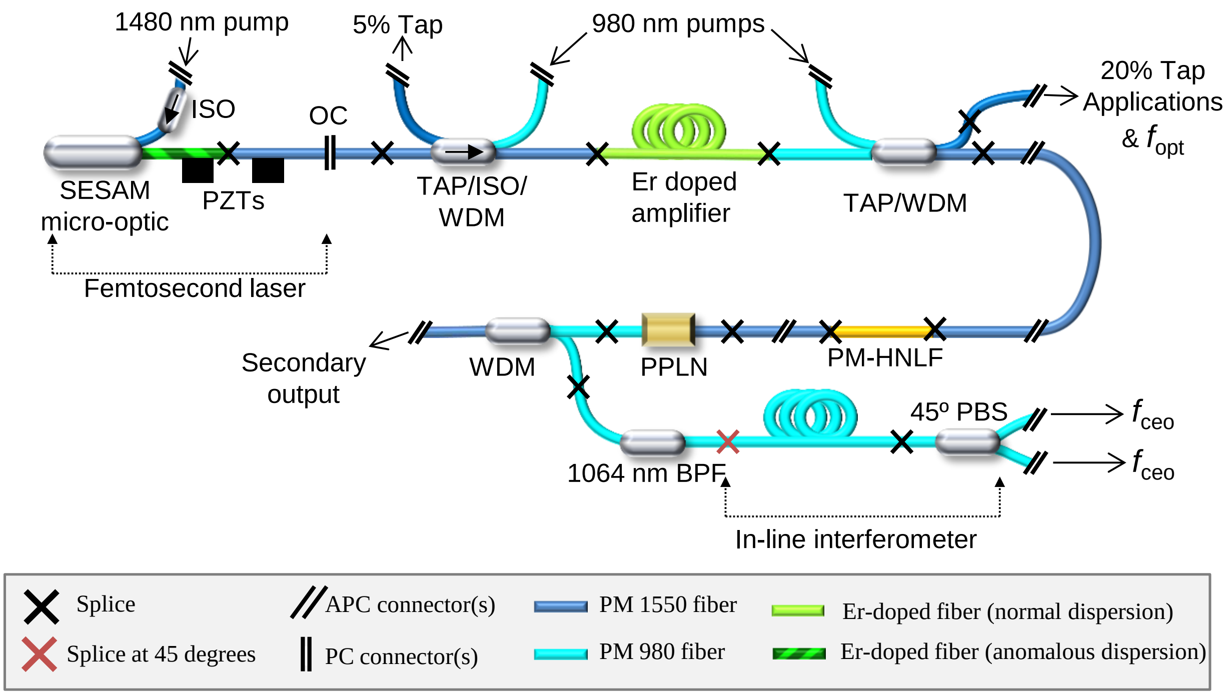

FIG 3. Detailed schematic of all-PM-fiber frequency comb. HNLF: highly nonlinear fiber, PPLN: periodically poled lithium niobate, OC: output coupler, ISO: isolator, WDM: wavelength division multiplexer, BPF: bandpass filter, PBS: polarizing beam splitter, PZT: Piezo-electric transducer, SESAM: Semiconductor saturable absorber mirror.

As shown in Fig. 3, the femtosecond laser described in the previous section has a 5 % tap to both monitor its output and to generate the repetition rate frequency, f_{rep}, signal. To overcome the relatively low-power and spectrally-narrow output from the laser, we use a nonlinear Er-doped fiber amplifier that both amplifies the 10 mW laser output to 300 mW and compresses the 200 fs pulses to a ~70 fs pulse width[61]. The amplifier consists of 1-2 meters of normal dispersion Er-doped fiber, necessary for the later pulse compression as described in Ref. 61, that is forward and backward pumped with 800 - 900 mW of 980 nm pump light. This Er-doped fiber is either a combination of low-gain (6 dB/m) fiber and high-gain (100 dB/m) fiber or solely high-gain fiber. Note that while the high-gain Er-doped fiber has a nominal core absorption of 100 dB/m at 1530 nm, its exact value can vary from spool to spool. Therefore, the Er-doped fiber length is set by optimizing the spectral width (or power) at the amplifier output. While the combination of high-gain and low-gain Er-doped fiber allows us to tune the amplifier dispersion independently of gain, in several more recent designs, we have found that use of only ~1.3 meters of high-gain Er-doped fiber is close to optimal and is simpler. A 20 % tap at the amplifier output redirects ~70 mW of comb light for applications. The remainder of the amplifier output (~220 mW) is compressed in 0.5 - 1.0 m of PM-1550 fiber, where the length is chosen to be a few centimeters short of maximal compression. These compressed pulses are then launched into 24 - 28 cm length of PM_HNLF to produce an octave-spanning spectrum shown in Fig. 4. The octave-spanning spectrum of Fig. 4b shows the strongly varying intensity typical of supercontinua produced via HNLFs[51,62–65]. The PM-HNLF used here had a nominal nonlinearity of 20 /W/km and a dispersion of 2.3 ps/nm/km at 1550 nm.[51]

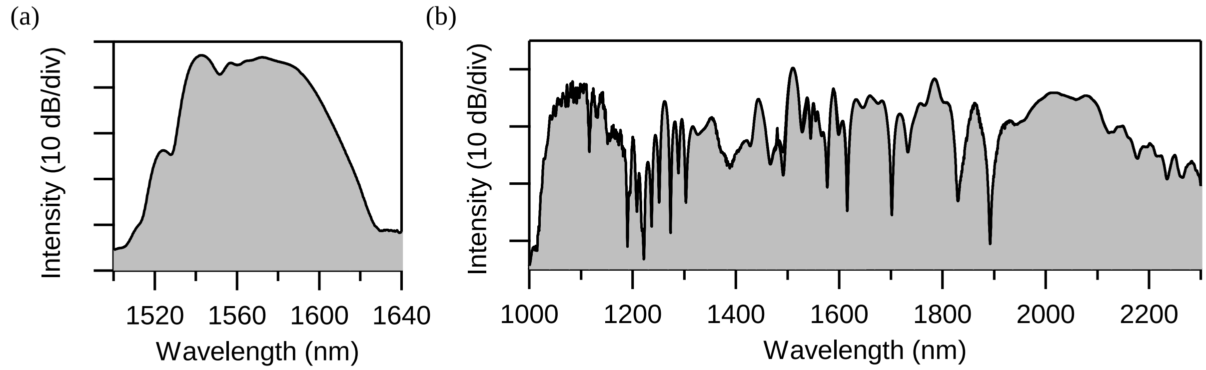

FIG. 4. Typical spectral outputs. (a) Spectrum after the amplifier with a ~ 50-nm full-width at half-maximum. At the input to the PM-HNLF, the average power is 220 mW and the pulse duration is ~70 fs. (b) Octave-spanning spectrum after the PM-HNLF.

In order to generate the f_{ceo} signal in the standard 1f-to-2f referencing scheme[66–68], the full octave-spanning spectrum is coupled through a commercial, fiber-coupled, ridged, PPLN waveguide, which frequency doubles the light at 2128 nm to 1064 nm.[69] This commercial waveguide has a built-in thermo-electric cooler to tune the PPLN temperature for optimized doubling at 2128 nm with a conversion efficiency of 5-10% including insertion losses and a bandwidth of ~ 3 nm (corresponding to a pulse duration of 0.4 ps for the doubled light pulse). As shown in Fig. 3, a wavelength division multiplexer (WDM) and narrowband 1064 nm filter select the fundamental and doubled ~1064-nm light pulses. f_{ceo} is the RF frequency from the heterodyne signal between the fundamental and doubled light.[66–68] (See Fig. 1b.)

However, detection of this heterodyne signal requires temporal overlap between the fundamental and doubled light pulses. This temporal overlap can be achieved by "fine tuning" the length of the PM fiber between the PM-HNLF and PPLN[45], but this approach is difficult given typical fiber lead lengths on the fiber-coupled PPLN waveguide. Therefore, we instead use an 'in-line' fiber interferometer that takes advantage of the differential delay between the fast and slow axes of a PM fiber.[49] The in-line interferometer is created by splicing the PM fiber output of the 1064-nm filter to a second PM fiber at a 45-degree rotation, which projects the fundamental and doubled light onto both fast and slow axes. After a suitable delay length, chosen to optimize the f_{ceo} SNR, the light from the slow and fast axes is recombined via a micro-optic polarizer oriented at 45 degrees. Typically the ratio of the fiber length in the in-line interferometer to the fiber length between the PM-HNLF and PPLN is about 10:1. The two outputs from the micro-optic polarizer contain the temporally and spatially overlapped fundamental and doubled light which are directed to a balanced detector to produce the f_{ceo} signal, shown in Fig. 5a.

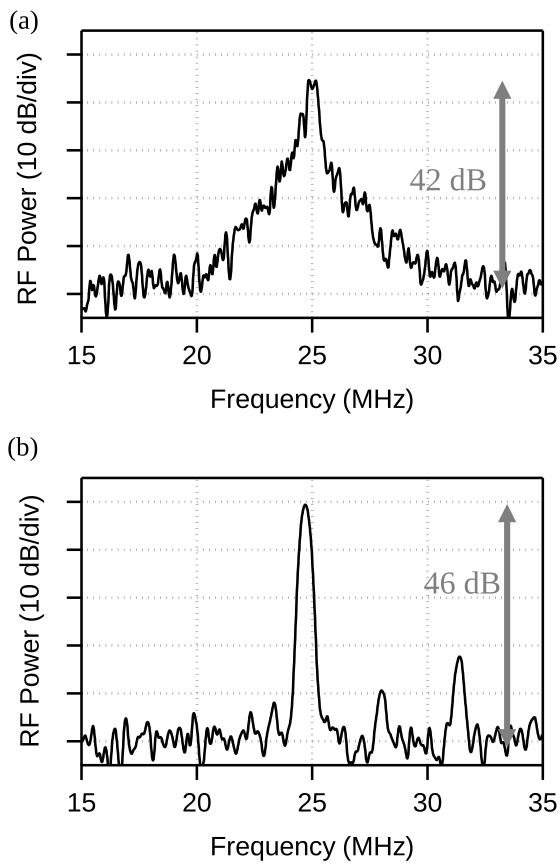

FIG. 5. (a) Free-running f_{ceo} heterodyne signal showing a 42 dB SNR in a 300 kHz resolution bandwidth (RBW). (b) Free-running f_{opt} heterodyne signal between the cavity-stabilized cw laser and nearest comb mode showing a 46 dB SNR in a 300 kHz RBW.

To fully stabilize the comb, we require a second measurement. As discussed in the introduction to this section, we stabilize the frequency of a single comb mode via a RF heterodyne measurement against a cavity-stabilized cw laser. Here, we use a cavity-stabilized laser at either 1535 nm or 1560 nm. These lasers could equally well be replaced by an optical clock, a robust portable cavity-stabilized laser[29], or even a freerunning diode laser[70] or fiber laser typical of dual-comb spectroscopy[16]. The comb light from the 20% tap is combined with this light in a 50/50 PM fiber combiner, filtered by a 0.5 nm-wide WDM, and detected to yield the RF signal shown in Fig. 5b. The RF frequency of this signal, f_{opt}, is the difference between the frequency of the cw laser and nearest comb mode. (See Fig. 1b.) Stabilization to cw lasers (optical standards) at wavelengths outside of the amplifier spectrum would require a modification of the optical design. For example, stabilization to a laser near 1 μm would require accessing some of the supercontinuum light prior to f_{ceo} detection, and stabilization at a visible wavelength might require a second fiber-coupled waveguide doubler, tuned to the appropriate wavelength, located at one of the outputs.

III. COMB STABILIZATION: PHASE-LOCKING f_{ceo} AND f_{opt}

A frequency comb can be stabilized either to an optical standard or via direct stabilization of the repetition rate to an RF standard. In either case, f_{ceo} is phase locked to a stable RF frequency. Here, we use optical stabilization, which is much more challenging but also yields higher performance than RF stabilization of the repetition rate. The challenge and improved performance stem from the fact that acoustic or mechanical perturbations to the laser will perturb the repetition rate but also cause the comb structure to breathe about ~0-1 THz.[44,71] Any changes in the repetition rate will be magnified by a factor of one million in the position of the optical comb mode, and therefore in the optical heterodyne signal against the cw laser. In other words, use of optical stabilization provides an enhanced "lever-arm" to detect these environmental noise effects. Full suppression of the noise in the optical domain has a corresponding multiplication in technical difficulty but leads to an optically-coherent comb with femtosecond-level residual timing jitter. Of course, if this level of performance is not required, the system described here could be easily reconfigured to directly phase lock the comb spacing, f_{rep}, to an RF standard.

Both f_{ceo} and f_{opt} are phase locked to RF frequencies derived from f_{rep}, which is known as full self-referencing.[72,73] The optical frequency of the n^{th} comb mode is then given by $\nu_n = \nu_{n0} + \frac{(n-n_0)}{n_0}(\nu_{n0} - f_{ceo})$ where ν_{n0} is the frequency of the comb mode at $n = n_0$ that is locked to the optical standard.[50] Note that this equation is not the usual $\nu_n = nf_{rep} + f_{ceo}$; rather f_{rep} is indirectly stabilized as $f_{rep} = (\nu_{no} - f_{ceo})/n_0$. Therefore, even if ν_{n0} is tightly stabilized to an optical standard, any noise on the f_{ceo} signal will lead to noise in f_{rep}. Here, the majority of the pulse-to-pulse timing jitter does in fact arise from the phase noise of f_{ceo}, which is best understood by visualizing the accordion-like motion of the comb modes about ν_{n0} in the frequency domain.[44,71] In that picture, it is also clear that the comb will have the highest optical coherence near $n = n_0$ and that coherence will degrade with increasing distance from this lock point. As shown in Section IV, for our system the optical coherence is preserved (less than one radian) over a bandwidth of ~ 110 to 200 THz, depending on the comb, centered about the mode at $n = n_0$.

We follow the now standard approach for stabilization of frequency combs, which implements a phase-locked loop around both f_{ceo} and f_{opt}. (See Fig. 6.) The RF frequency, f_{ceo}, is phase-locked via feedback to the pump laser current of the femtosecond laser and the RF frequency f_{opt} is phase-locked via feedback to the cavity length, which is controlled through a "slow" and a "fast" piezoelectric transducer (PZT) bonded to the intracavity fiber. Figure 6 shows the overall system. As with any phase-locked loop, the two critical parameters are a large dynamic range (to avoid phase-slips) and a large feedback bandwidth (to suppress noise). In the past, we have used conventional op-amp-based analog control-electronics. Here, we focus on two critical improvements to our previous approach: (i) the implementation of digital signal processing for the phase lock and (ii) a standardized design for high-bandwidth cavity length control through a PZT bonded to the fiber. We first discuss the digitally-based feedback control and then the PZT design.

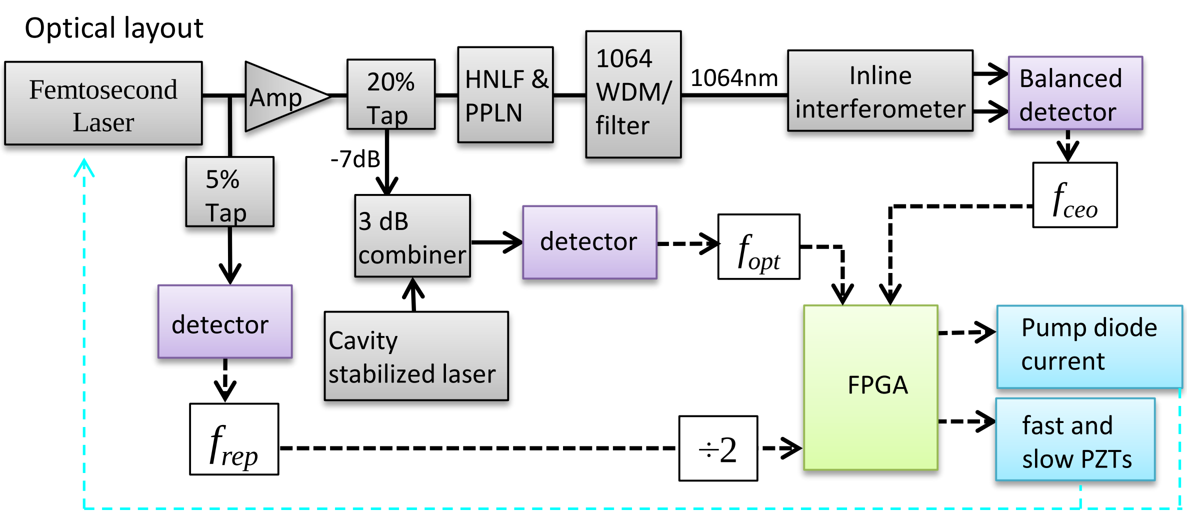

FIG 6. Schematic of the fully phase-locked frequency comb. PZT: piezo-electric transducer, FPGA: field-programmable gate array.

A. Field-Programmable Gate Array (FPGA) based Digital Control

Digital control and real-time digital signal processing implemented on FPGA platforms have enabled significant advances for both real-time processing of frequency comb signals[12,70] and phase-locking of ultra-stable cavity-stabilized cw lasers[30,74], overcoming many drawbacks inherent to conventional analog systems. Specifically, digital processing allows for the unwrapping and continuous tracking of phase excursions of 10^6 radians or more, rather than the $\pm\pi/2$ limit imposed by an analog phase-detector. This continuous tracking protects against phase-slips from environmental perturbations. In addition, the system has improved immunity to electro-magnetic interference

(EMI) because the raw detector signals for the f_{ceo} and f_{opt} heterodyne beats are digitized immediately after an RF anti-aliasing filter, and the digital processing is noise-free until generation of the analog control-signal in a digital-to-analog converter (DAC). The digital system, of course, allows for simple fine-tuning of loop parameters as well as easy adjustments of the lock frequencies and filter bandwidths. Finally, while not implemented here, more sophisticated state observer-predictor control methods would further increase robustness. These advantages do require expertise in FPGA programming to implement the digital signal processing algorithms. Here, we seek to provide a high level view of the processing and control algorithms that could be implemented on a range of digital processing platforms. The exact details will depend on the platform and is therefore beyond the scope of this paper.

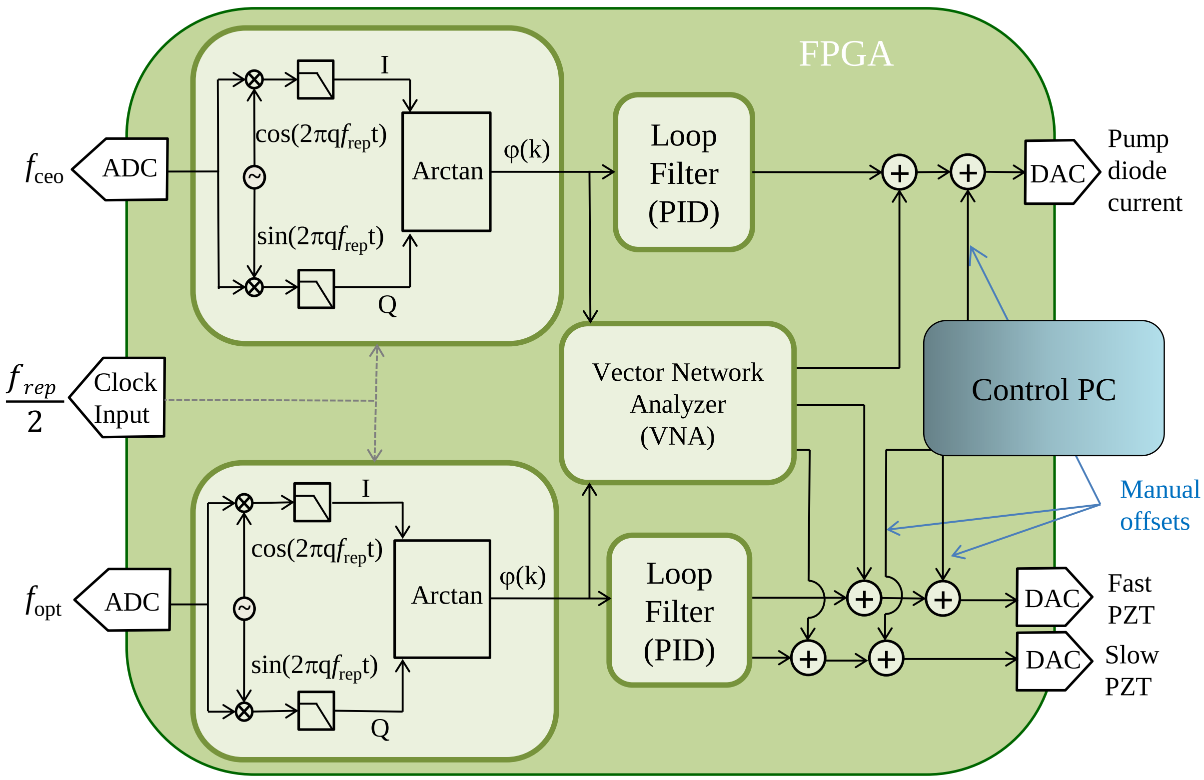

FIG. 7: Overview of FPGA-based digital control. ADC: Analog-to-Digital Converter, DAC: Digital to Analog Converter, PID: Proportional Integral Derivative.

Figure 7 provides a basic outline of the FPGA-based control system, which consists of input analog-to-digital converters (ADCs), an in-phase and quadrature (IQ) detection module for detection of the phase, a loop filter, output DACs, and built-in real-time diagnostics through zero-deadtime frequency counters, phase-noise analyzers, and a vector network analyzer (VNA) for transfer function measurements. This is currently implemented with hardware originally designed for locking cw lasers to ultra-stable optical cavities[30,74] and consists of a custom analog input/output daughterboard and an OpalKelly XEM integration module with Xilinx Spartan-6.[75] The two 16 bit, dc-coupled ADC inputs operate with a 50 MHz input bandwidth and 100 MS/s. One 16-bit DAC output is used for the pump diode current control and two 16-bit DACs are used for the PZT control, one of which (the "slow PZT output" in Fig. 7) is a 0-64 volt output. The FPGA is clocked directly from half the repetition rate, enabling self-referenced operation. Standard digital-signal-processing routines are implemented, as described qualitatively below.

The RF signals f_{ceo} and f_{opt} are digitized and mixed down via IQ detection against the phase-lock frequency, qf_{rep} (which is in general different for the two phase locks). For a fully self-referenced system, this lock frequency, qf_{rep}, is derived from f_{rep} and q = M/N, where M is any integer and $N=2^{48}$. The phase of the baseband signal is calculated using an arctangent operation and unwrapped (not shown in the diagram) to $\pm$ 3x10^6 radians of linear range, which allows linear behavior even under significant perturbations. As long as frequency/phase excursions caused by environmental perturbations to the frequency comb do not exceed the input filter bandwidth (25 MHz in this work), they are tracked and the phase is recovered without 2π ambiguities. The loop filter which follows the phase unwrapping operation is a tunable proportional-integral-derivative (PID) filter.

A built-in VNA allows for measurement of transfer functions and real-time monitoring of residual lock phase-noise. When desired the VNA can provide a small dither to any of the output signals to measure the transfer function of any given modulator in the frequency comb or to measure the sign of optical or CEO beats (to determine if the cw laser above or below the comb tooth in the f_{opt} signal, for example). During normal operation the dither is off and the VNA is passively monitors residual phase noise on the locks. The FPGA also has implemented two zero-deadtime, triangular averaging frequency counters operating at a 1-s gate time to monitor the long-term performance.

(a)

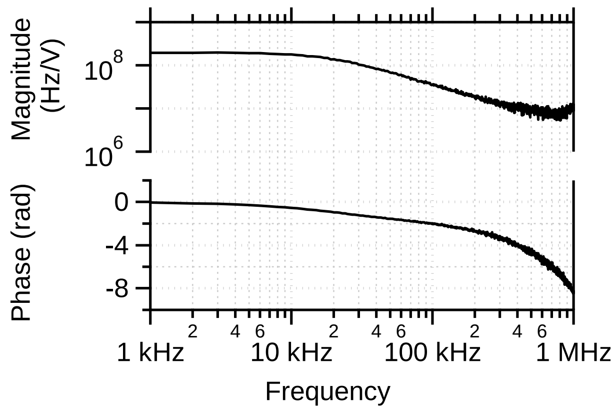

(b)

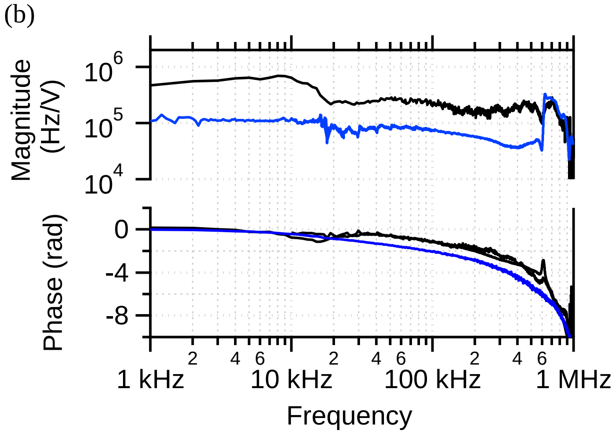

FIG. 8. (a) Transfer function of the pump-diode power control for f_{ceo} showing the first order pole leading to a roll-off at ~ 20 kHz associated with the femtosecond fiber-laser gain response. (b) Transfer function of the "fast" PZT to control f_{opt}, showing the flat response out to ~ 100 kHz for both the "free-standing" (black line) and "pocket-clamp" (blue line) PZT mounting methods (discussed in Section III.B). Note the latter has a stronger bare PZT resonance at 700 kHz, which limits the phase-locking bandwidth.

The phase-lock performance is determined by the feedback bandwidth. The transfer functions for feedback to both f_{ceo} and f_{opt} are shown in Fig. 8. The response of f_{ceo} to pump diode power has an intrinsic pole at ~ 20 kHz associated with the gain of the Er-doped fiber.[59,76] The derivative term in the PID loop compensates for this pole and extends the feedback bandwidth to ~100 kHz, at which point it is limited by the bandwidth of the current controller and a second pole originating from the femtosecond laser dynamics. For future systems, inclusion of fast small intracavity loss modulators, such as graphene modulators grown onto the SESAM, could provide even higher feedback bandwidths for f_{ceo}.[77] Feedback to control f_{opt} is achieved via tuning of the femtosecond laser cavity length through two PZTs glued to the intracavity fiber, the specifics of which are discussed in the next section. The stabilized RF signals of f_{ceo} and f_{opt} are shown in Fig.9 and the residual noise is discussed in detail in Section IV.B.

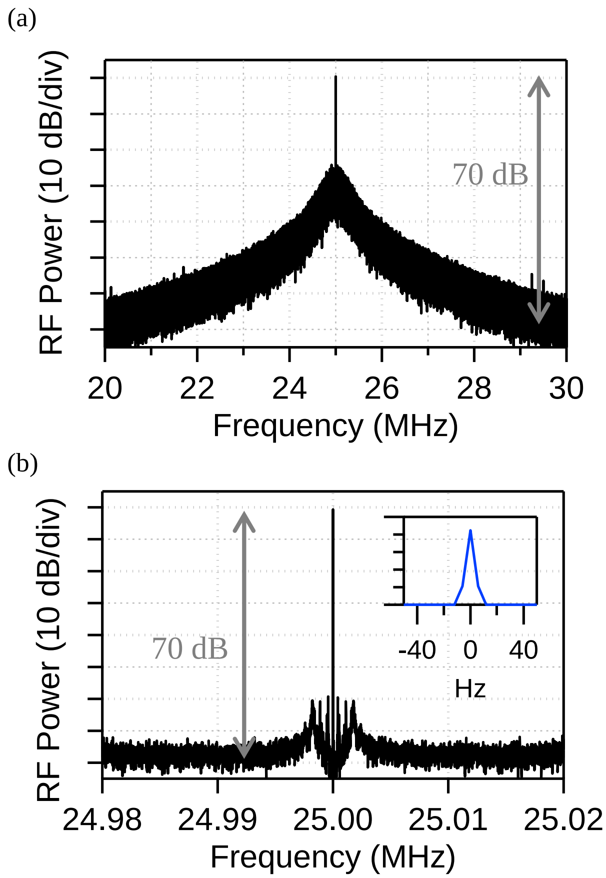

FIG 9. (a) Phase-locked f_{ceo} signal for comb "A" in a 6 Hz resolution bandwidth (RBW). (b) Phase-locked f_{opt} signal for comb "A" in a 6 Hz RBW. The inset shows that the linewidth is limited by the 0.3s acquisition time.

B. Femtosecond Laser Cavity Length Control

In order to stabilize f_{opt}, feedback is applied to adjust the femtosecond laser cavity length via fast and slow PZT fiber-stretchers. The fast PZT fiber-stretcher modulates the cavity length with up to 100 kHz of feedback bandwidth while the slower (< 1kHz bandwidth) long-travel PZT provides a larger dynamic range corresponding to ~ 600 MHz on f_{opt}. Both PZTs are glued to the 250 μm cladding-diameter intracavity Er-doped fiber or PM 1550 fiber with consumer-grade 5-minute epoxy.

For phase locks based on PZT fiber-stretchers, the feedback bandwidth is typically limited by phase-shifts associated with mechanical resonances. While the bare PZT stack has resonances at 700 kHz and higher frequencies, the mounting of the fiber to the PZT potentially induces resonances at much lower frequencies, on the order of 10 kHz. In order to damp these resonances, care must be taken in the exact PZT-fiber mounting geometry. We achieve 100 kHz bandwidth for our fast PZT fiber-stretcher using two different mounting approaches (see Fig. 10): a free-standing scheme and a pocket-clamping scheme.

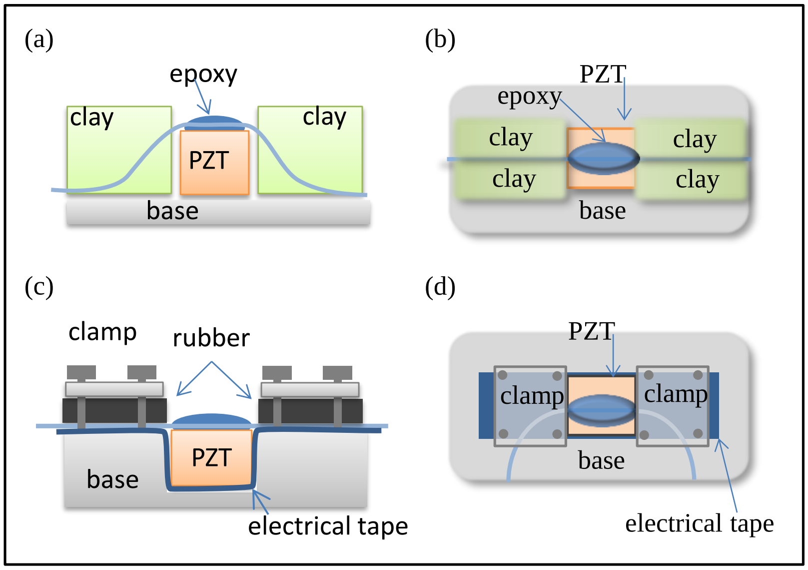

FIG. 10. Methods of mounting a small PZT to achieve high feedback bandwidth. (a) Free-standing scheme side view. The ~ 2 cm radius of curvature arc is created as the fiber travels from the top of the PZT to the laser baseplate. The electrical leads (not shown) are attached to the side of the PZT. (b) Free-standing scheme top view. (c) Pocket-clamping scheme side view. The electrical leads (not shown) are attached to the side of the PZT and emerge vertically out of the pocket. (d) Pocket-clamping scheme top view. The in-plane ~ 2 cm radius of curvature arc is formed when the fiber is clamped onto the baseplate.

For both mounting schemes, the fiber (encased by its 250 μm buffer) is epoxied along the axis of a 2 mm x 2mm x 2mm stack PZT. This attachment of the fiber results in a total fiber stretch that is approximately one-tenth the total PZT throw. It is critical that there remains an arc in the fiber as it leaves the PZT surface in order to preserve the dynamic range of the fiber-stretcher by preventing fiber compression. However, the “violin”-like resonances between 1 kHz and 100 kHz must be damped. In the free-standing design, the a tight, ~ 2 cm radius of curvature, arc arises naturally as the fiber travels from the top of the PZT to the laser baseplate. Resonances in the suspended fiber are damped with modeling clay pressed up against the fiber on both sides. The modeling clay is surprisingly robust and has maintained excellent damping properties even after being vibrated on a shaker table in Ref. 49. The downside of this approach is that the best damping performance does require significant user adjustment.

In the pocket-clamping scheme (Fig. 10b), the PZT held in a small pocket and the ~ 2 cm radius fiber arc is in the horizontal plane of the laser baseplate. To avoid resonances, the two fiber arcs sit upon a double layer of electrical tape attached to the baseplate. The fiber is clamped from above with a 2-mm-thick stiff rubber piece and thin 1.27-mm-thick aluminum clamping plate, while monitoring the PZT transfer function in real time. Unsupported fiber is very prone to resonances, so the size of the PZT pocket does not exceed 2.9 mm for the 2-mm-long PZT used here. We find that the PZT should not be attached to the baseplate. While the pocket-clamping method is more straightforward and repeatable than the free-standing method, the bare PZT resonance at 700 kHz is stronger (see Fig. 8) and can limit the bandwidth. However, the servo bandwidth can still reach 100 kHz even with this limitation. Higher feedback bandwidths have been achieved using an intracavity electro-optic modulator (EOM)[46,54,78,79], with bandwidths as high as 4 MHz.[79] However, EOMs are expensive, have high third order dispersion, inconveniently located fixed-points and add intracavity loss. A high bandwidth PZT is a very attractive, low cost option for many applications.

The low bandwidth PZT can be mounted with far less effort as it is only driven at frequencies below 1 kHz. The fiber is epoxied to the PZT in the same manner as the fast PZT but no pocket is required and the PZT rests on the laser base with the fiber running over the top and gently arcing back down to the baseplate. The fiber and PZT are secured to the baseplate with tape and epoxy. Similar to the fast PZT, the total stretch induced in the fiber for the slow PZT is about one-tenth of the total PZT throw.

Finally, active thermal control of the femtosecond laser cavity length is necessary for operation in uncontrolled environments because the optical path length of the cavity fiber shifts by ~10 ppm/°C. Given the dynamic range of the slow PZT fiber stretcher, the temperature of the cavity fiber must remain within 0.3 °C. (A 0.1 °C change corresponds to a 200 MHz shift in $f_{opt.}$) Therefore, thermo-electric coolers (TECs) are placed underneath the aluminum box that houses the femtosecond laser and amplifier (see Appendix C). We control the aluminum box temperature based on an internal thermistor. For long term operation we implement a third control loop that adjusts the temperature set point to keep the slow PZT within its dynamic range. For environments with limited temperature and humidity regulation, this third stage of control is critical.

IV. PERFORMANCE

In this section, we present the performance of combs A, B, and C, all of which have been in continuous operation for at least seven months. During that period, they have routinely operated on a wheeled cart near open windows from summer to winter demonstrating their ability to operate outside the well-controlled metrology laboratory. For these three combs, we have found that output power, spectral shape and center wavelength vary little between them. Comb B does have a slightly higher intrinsic f_{ceo} phase noise. Therefore, its estimated pulse-to-pulse timing jitter is higher and its projected coherence bandwidth is lower as discussed in Section IV.B. Table I presents a summary of various performance metrics for the three combs.

All the performance parameters given here – the phase noise, timing jitter, and frequency noise – are "residual", "in-loop" values. By residual, we mean that the values are all with respect to the underlying "clock", which in this case is the cavity-stabilized laser. This cavity-stabilized laser will drift as the optical cavity length changes and it has no absolute stability in the sense of a true atomic clock. By "in-loop", we mean the quantities are measured from the same signals used to phase lock the comb. There is no separate, second comb against which the performance was evaluated. (In Ref. 49, we did compare the comb mode linewidth to a second cavity stabilized laser to verify the overall comb linewidth was sub-Hz.) In general, such residual, in-loop values represent an upper limit to the frequency comb performance. In any experiment, there will be varying path lengths and other effects that can degrade the comb light that is ultimately delivered to the experiment. As a result, comb-based experiments are typically designed to minimize these effects in order to achieve the best possible performance.

TABLE I: Comb Performance. (See also Section IV.B)

Property	**A**	**B**	**C**
Femtosecond Laser Center Wavelength (nm)	1563.6	1558.8	1560.0
3 dB Femtosecond Laser Width (nm) [Equivalent Pulse Width (fs)]	12.2 [210]	11.5 [222]	12.6 [202]
3 dB Amplifier Width (nm)	54	52	51
20% Amplifier Tap Output Power (mW)	~70	~70	~70
f_{ceo} Integrated Phase Noise[a] (rad) 10 MHz to 6 Hz	2.0	3.6	2.6
f_{opt} Integrated Phase Noise[a] (rad) 10 MHz to 6 Hz	0.12	0.14	0.15
Estimated Pulse-to-Pulse Timing Jitter[a] (fs)	1.6	2.9	2.1
Projected Coherence Bandwidth[a] (THz)	200	110	150

a All phase noise parameters here are residual, "in-loop" values so the coherence is with respect to the reference oscillator.

A. Long term phase coherence

A significant limitation on comb stability is caused by a phase unwrapping error, i.e., a phase-slip. Phase-slips can be driven by two processes: (i) environmental perturbations that cause the heterodyne signal to momentarily exceed the signal processing filter bandwidth, *BW*, and (ii) limited SNR that causes a (nearly) 2π error in the phase calculation. The larger the filter bandwidth used to process the signal, the lower the probability of an "environmentally driven" phase-slip. However, too large a filter bandwidth will decrease the SNR and ultimately lead to "SNR-driven" phase-slips.

The probability of this SNR-driven phase-slip can be calculated to determine the optimal filter bandwidth. For a signal with additive white Gaussian noise, this phase-slip rate is given by $\frac{1}{2} BW \times \mathrm{erfc}\left(10^{SNR/20} / \sqrt{2}\right)$, where *erfc* is the complimentary error function, and the SNR is in dB for the given filter bandwidth.[80] Note that this is very similar to computing the bit-error-rate for binary-phase-shift-keying (BPSK). To verify that this expression accurately describes our system, we applied white electrical noise to the f_{ceo} signal before it entered the digital-locking electronics and monitored the un-degraded signal with a separate frequency counter to measure the phase-slip rate. A frequency jump on an independent frequency counter was recorded as a phase-slip when it exceeded a 1 Hz change from the mean frequency. In addition, we performed a simulation by adding Gaussian noise to a previously recorded high SNR f_{ceo} signal and simulating the digital processing to find the resulting phase slip rate. Both the measurement and the simulation results match the formula given above as shown in Fig. 11.

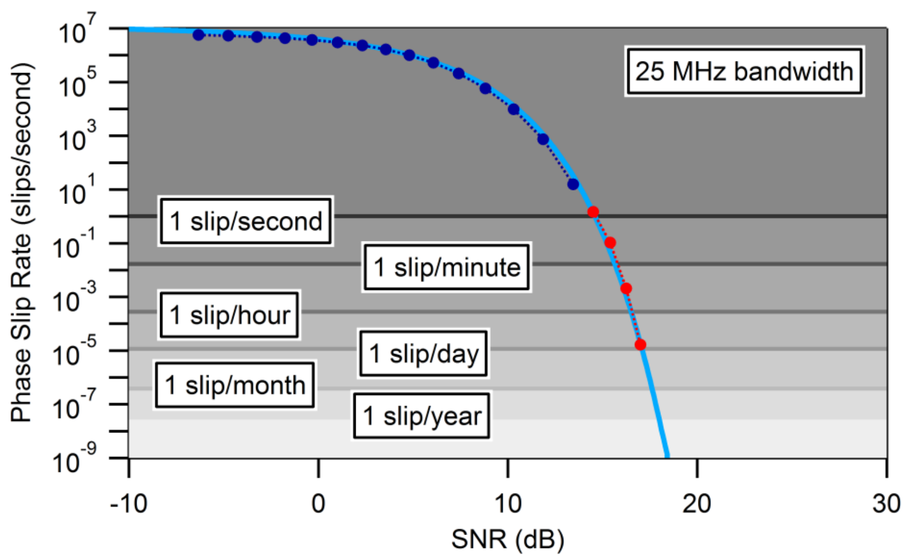

FIG. 11. The rate of phase slips versus SNR of the f_{ceo} signal at a fixed processing bandwidth of 25 MHz. Measurements of the rate were taken by mixing in white noise to the signal and monitoring the system for phase slips (red points), as well as by adding noise to a pre-recorded f_{ceo} signal (dark blue dots). The measurements and simulation agree with the analytical calculation assuming Gaussian noise (light blue curve). In our comb operation, the SNR is typically ~35 dB in a 25 MHz bandwidth resulting in a negligible rate of phase-slips.

From Fig. 11, it is clear that the rate of SNR-driven phase-slips is a very strong function of the SNR and, therefore, filter bandwidth (since SNR$\propto$1/bandwidth). An SNR of 20 dB is required for long-term phase-slip-free operation. However, operation close to the 20 dB SNR limit results in a sensitivity to slight changes in power, noise floors, or transient RF pick-up as they will cause a reduction in SNR and thus potentially a phase-slip. Here we operate at an SNR of 25 – 35 dB, achieved in a 25 MHz filter bandwidth, for both the f_{ceo} and f_{opt} signals.

Figure 12 shows the long term stability of a locked comb, which operated fully-stabilized without phase-slips for 91 hours until the measurement was stopped as the combs were needed for other projects. The improved long term performance, relative to Ref 49, comes largely from the implementation of the digital control. Phase-slip free operation over extended periods should enable time-based clock comparisons and synchronization of clocks over long timescales via optical free-space time transfer where phase-slips are deleterious.[28]

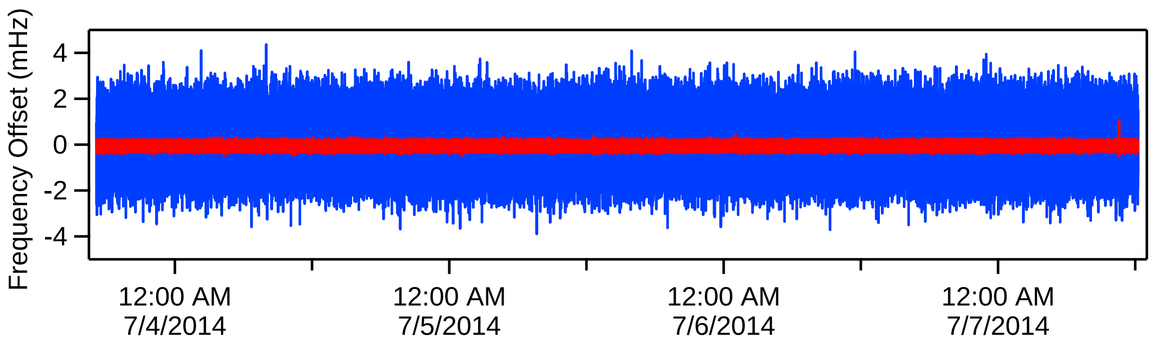

Fig. 12. Long-term stability of the combs. Counted offset of f_{ceo} (blue) and f_{opt} (red) signals from their lock frequencies with a 1 sec gate time for comb "B". The standard deviation for f_{ceo} is 0.9 mHz and for f_{opt} is 0.1 mHz. There were no phase-slips over the 91 hours of the measurement (as evidenced by the lack of > 1 Hz frequency excursions).

B. Phase Noise and Timing Jitter

The phase-noise spectra, shown in Fig. 13, provides a measure of the performance of the combs on short timescales. For the three combs, the integrated phase-noise for f_{opt} ranges from 0.12 – 0.15 rad from 10 MHz to 6 Hz and for f_{ceo} ranges from 2.0 – 3.6 rad from 10 MHz to 6 Hz with values extrapolated to Nyquist at 100 MHz of 0.16 - 0.23 rad and 2.0 - 3.6 rad, respectively. (Note that the sub-radian phase noise for f_{opt} results in the sharp coherent peak in the RF signal shown in Fig. 9b, while the 2 rad phase noise for f_{ceo} of comb "A" results in a coherent peak on top of a broader background in the RF signal shown in Fig. 9a.) For all of these combs to achieve the lowest phase noise, the femtosecond laser was pumped to just below the point of cw breakthrough, i.e. the pump power at which the output spectrum shows a narrow frequency spike, corresponding to a cw mode, in addition to the broad frequency spectrum of the comb.

The comb is optically coherent around the optical lock point at 1535 nm. For many applications, it is important that this optical coherence extends across all comb modes. We define the projected coherence bandwidth as the frequency range centered at the optical lock point for which the phase noise on the comb modes remains below one radian. Here the 2.0 to 3.6 rad phase noise on f_{ceo} coresponds to a projected coherence bandwidth across the comb spectrum of 200 to 110 THz. This means that the entire 150 THz-wide (1 µm-2 µm) comb output, centered at the ~195-THz optical lock point, is coherent in most cases. Based on these numbers, even if the optical lock point were shifted to 1070 nm for an Al^+ ion clock[81] or 1156 nm for a Yb clock[82], the telecommunication bands at 1550 nm used for free-space time and frequency transfer[28] would still be optically coherent.

The pulse-to-pulse timing jitter is calculated from the phase noise at the f_{ceo} and f_{opt} lock points divided by the angular optical frequency separation, or for comb A, $\sqrt{2.0^2+0.16^2}/(2\pi\times 195\ \mathrm{THz}) = 1.6$ fs, assuming uncorrelated noise. For the noisier comb B, this jitter increases to 2.9 fs of pulse-to-pulse timing jitter. In all cases, because of the tight optical lock, the dominant source of pulse-to-pulse timing jitter is the residual phase-noise on f_{ceo}. (See the lock point diagram in Fig. 1b. and discussion in Section III.)

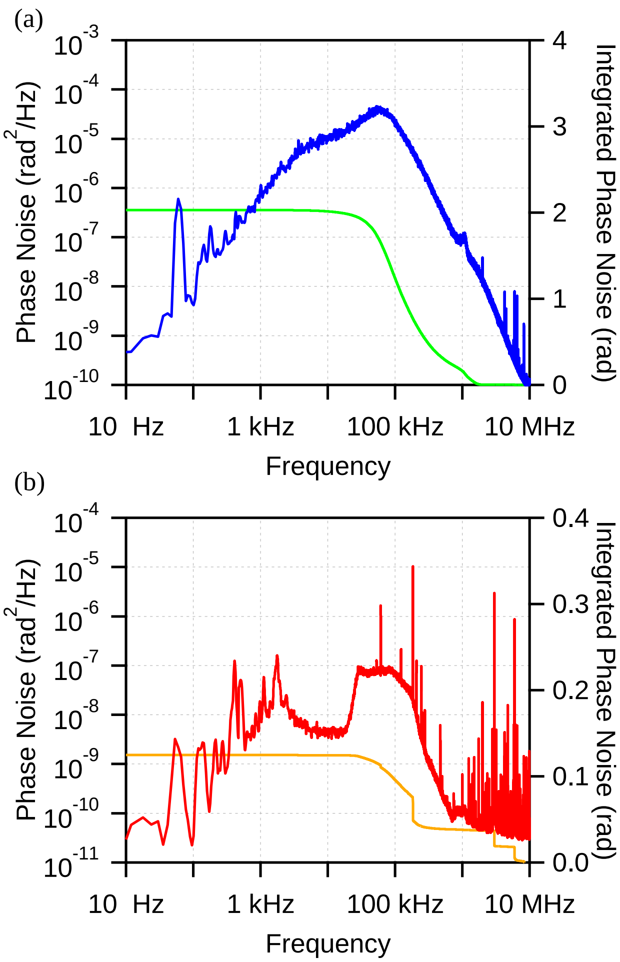

FIG. 13. (a) f_{ceo} phase noise (blue, left axis) and integrated phase noise (green, right axis) from 10 Hz to 10 MHz for comb "A". (b) f_{opt} phase noise (red, left axis) and integrated phase noise (orange, right axis) from 10 Hz to 10 MHz for comb "A".

VI. CONCLUSIONS

We have developed a self-referenced all-PM-fiber frequency comb design capable of coherent operation outside of a well-controlled laboratory setting within a small liter-volume optics package. Multiple frequency combs have been constructed and tested. With the use of digitally-based control and ~100-kHz closed-loop bandwidths, the combs operate with in-loop optical frequency uncertainties of <1 mHz at one second, more than sufficient for use with optical clocks.[83] We have also shown that these combs operate with no phase-slips for 91 hours. Finally, the residual 1.6 – 2.9 fs timing jitter is comfortably below the ~ 10 fs timing jitter acceptable for most precison comb applications such as optical time transfer, LADAR, and comb spectroscopy.[5–28] It is hoped that this optically coherent and robust comb design will facilitate "real-world" applications of these metrological tools.

ACKNOWLEDGEMENTS

We acknowledge assistance in comb fabrication and design from Ron Hui, assistance in digital–control design from David Leibrandt, and helpful discussions with Tara Fortier, Gabe Ycas, and Marla Dowell. This work was funded by the DARPA PULSE program and the National Institute of Standards and Technology (NIST).

APPENDIX A: CRITICAL FIBER LENGTHS

Fabrication of an octave-spanning comb requires the use of specific fiber lengths. Critical fiber lengths are given in Table II with the corresponding Fig. 14 illustrating their location. The lengths given are for the specific fiber types listed; however, other gain fibers or highly nonlinear fibers could be used with the appropriate adjustment in length as necessary.

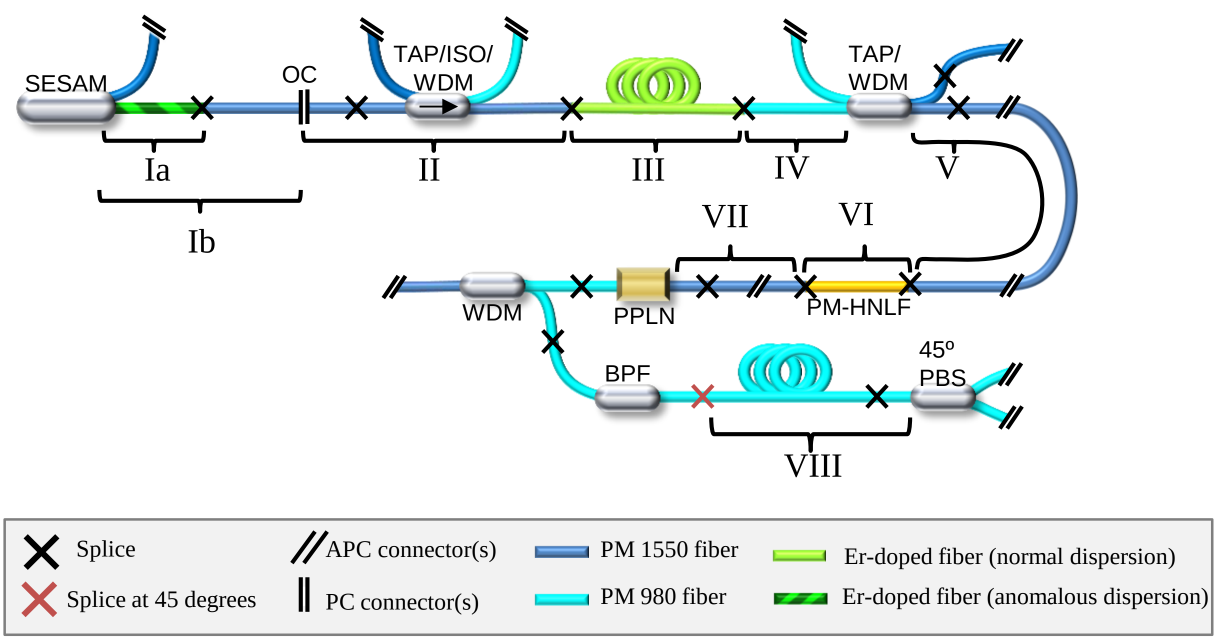

FIG 14. Schematic of comb for determining critical fiber lengths. Critical fiber lengths are given in Table II. ItFor the second WDM, the default fiber is PM980 on the common port, as noted in the figure. However, it is unlikely the use of PM980 or PM1550 is critical here

TABLE II. Critical fiber lengths for three fully-characterized combs. All lengths are given in centimeters.

Section of Comb	A	B	C
Ia Gain medium: anomalous dispersion Er-doped fiber (Nufern PM-ESF-7/125[75])	16.0	16.5	8.5
Ib Total fiber in femtosecond laser cavity	50.0	50.0	50.0
II. Between output coupler and amplifier (PM-1550)	49	44	49
III. Gain medium: normal dispersion Er-doped fiber (OFS EDF08-PM and nLight Er80-4/125-HD-PM[75])	228.5[a]	243.0[b]	228.5
IV. Compression between amplifier and PM-HNLF (PM-980)	42	42	42
V. Compression between amplifier and PM-HNLF (PM-1550)	68.5	69.0	105.0
VI. PM-HNLF (2.3 ps/nm/km @1550 nm)	24.5	27.5	27.0
VII. PM-1550 between PM-HNLF and PPLN	52.0	48.5	43.5
VIII. Delay length in in-line interferometer (PM-980) [c]	544.5	500.0	388.0

[a] This consists of 70 cm low gain Er-doped fiber followed by 158.5 cm of high gain Er-doped fiber
[b] This consists of 80 cm low gain Er-doped fiber followed by 163 cm of high gain Er-doped fiber
[c] Generally the fiber length ratio of VII to VIII will be about 1:10

APPENDIX B: OUTPUT COUPLER DESIGN

A range of output couplers have been tried in this laser design. Reflections at 1560 nm have ranged from 80% to 90% with combs A-C all using an 80% which provides additional output power with no other observable change in performance. (See Fig. 15) Couplers at 75% have been tried as well but mode locking was unstable although such couplers might work with a higher modulation depth SESAM. We have used standard commercial dielectric coatings applied to the bare end of an FC/PC connector from several coating suppliers using an array of processes. Generally speaking the durability of the coating is not a critical requirement as it only ever experiences compressive force. We have however found that providing a coating supplier with FC/PC ends that have had the boots removed and have only a 250 μm buffer on the pigtail does reduce outgassing and leads to a higher yield on the coating.

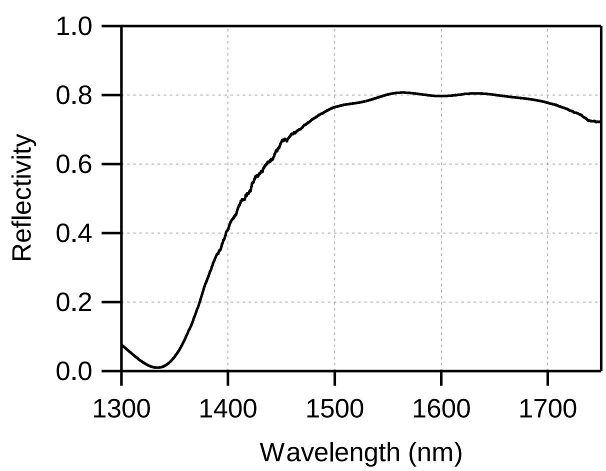

FIG 15. Reflectivity curve of a typical dielectric coating.

APPENDIX C: CAVITY FABRICATION AND PRECISE SELECTION OF THE FEMTOSECOND LASER REPETITION RATE

Many applications, such as high-precision spectroscopy, time-frequency transfer, and microwave generation, require a femtosecond laser with a precisely defined repetition rate.[28,53,54] Unlike many laboratory-based frequency combs, which can rely on a free-space variable delay-line for coarse repetition-rate tuning[40,84], the all-fiber design must have the optical path length set during comb fabrication. The repetition rate can be fine-tuned by changing the temperature of the femtosecond laser fiber (10 ppm/°C). However, it is necessary to have the total cavity length constructed within a few parts in 10^5 of the targeted path length for operation at reasonable temperatures. (One part in 10^5 translates to 5 μm for a 200 MHz linear cavity.)

We use a two-step approach to realize the desired repetition rate during construction of the femtosecond laser cavity. (See Fig. 16) In the first step, the length of the two halves of the laser cavity (the micro-optic assembly with Er-doped fiber pigtail on one side and PM-1550 fiber pigtail with FC/PC on the other side) are measured and co-aligned in a fiber fusion-splicer, but not actually spliced. In order to measure the round-trip cavity delay time, light from a coherent optical frequency-domain reflectometer (OFDR) is coupled into the cavity via the FC/PC connector. The OFDR signal returns the time delay or optical path length between the PC-connector interface at the near end of the femtosecond laser cavity and the SESAM on far end, see Fig. 16b. Our comb-calibrated OFDR was originally developed for LADAR applications[25,27,85], and is capable of measuring range-resolved optical reflections in the femtosecond laser cavity at a resolution of 0.4 ps (130 μm) and a precision level of 1 fs. In general this approach of optical length measurement could be reproduced with any high-end, commercially available OFDR.[86]

Once the optical path length of the cavity has been determined, the appropriate length of fiber is removed via cleaving and the fibers are spliced together. Typically, this is an iterative process. In the first pass, the cavity is left deliberately too long to allow for multiple cutbacks with OFDR measurements after each. Note that the OFDR returns the round trip travel time in the cavity to ~ 1 fs, which directly gives the repetition rate. However, the cleaving length requires knowledge of the index of the cavity, which can easily be determined by the series of cutbacks. With care, one can achieve an optical cavity that is within 100 μm of the desired length, yet also deliberately longer than the desired value.

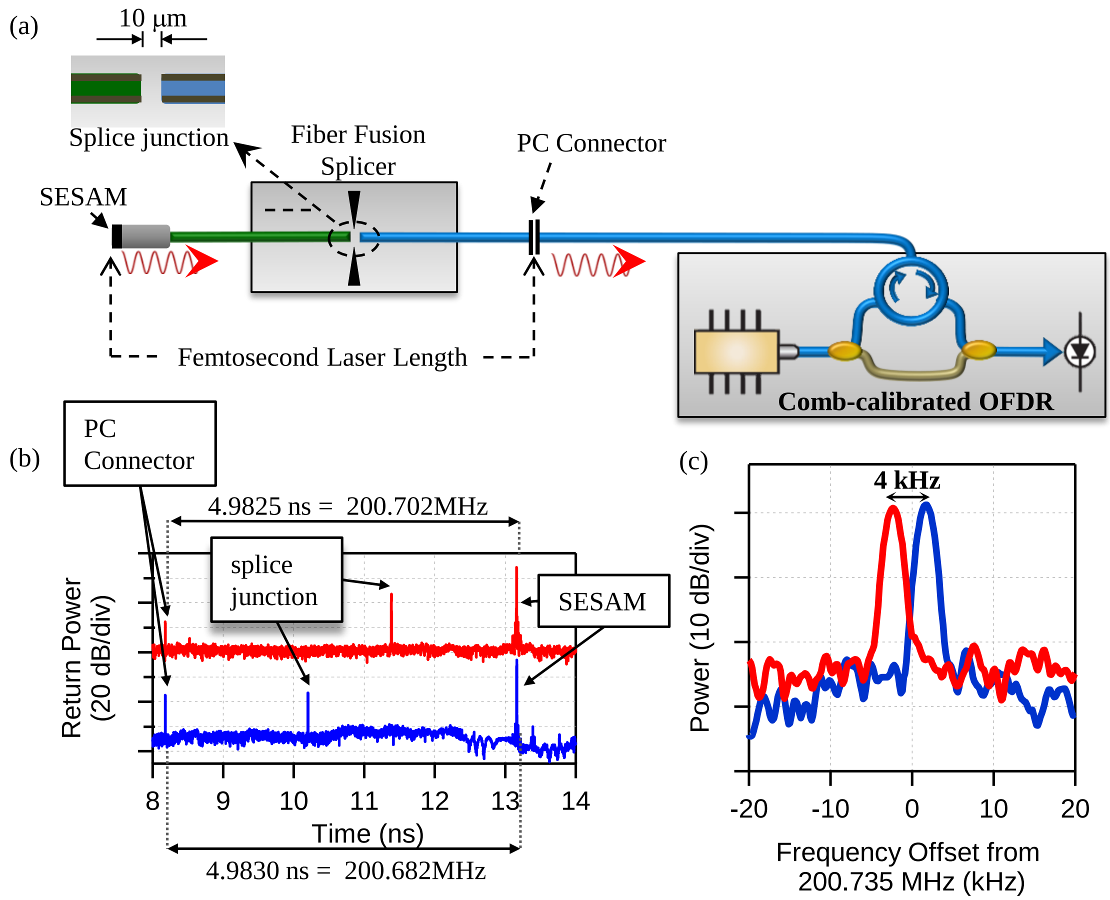

FIG 16. (a) Setup to measure and adjust the femtosecond laser cavity length/repetition rate during fabrication. A comb-calibrated optical frequency-domain reflectometer (OFDR) measures the round trip delay in the cavity between reflections coming from the SESAM and the PC connector interface. (b) OFDR signals from two different femtosecond lasers. Each peak corresponds to a reflection in the cavity with a time axis that is relative to a reference arm. Absorption due to the Er-doped fiber in the cavity reduces the height of the SESAM peak. Curves are offset for clarity. (c) Repetition rate for a pair of femtosecond lasers constructed using this technique after fine-tuning of the repetition rate via polishing showing the desired 4 kHz repetition rate separation.

In the second fine-tuning fabrication step, the PC-connector at the end of the femtosecond laser cavity is polished. Using standard diamond polishing paper, it is possible to remove the remaining excess cavity length in a controlled fashion. As the cavity is already constructed, one can periodically measure the repetition rate by mating the newly polished end with the dielectric output coupler and pumping the cavity. With some iteration the cavity length can be tuned within 10 µm of the desired length. For a 200 MHz cavity, one can achieve the desired repetition rate with less than 2 ^{o}C of temperature tuning applied to the femtosecond laser.

APPENDIX D: PACKAGING

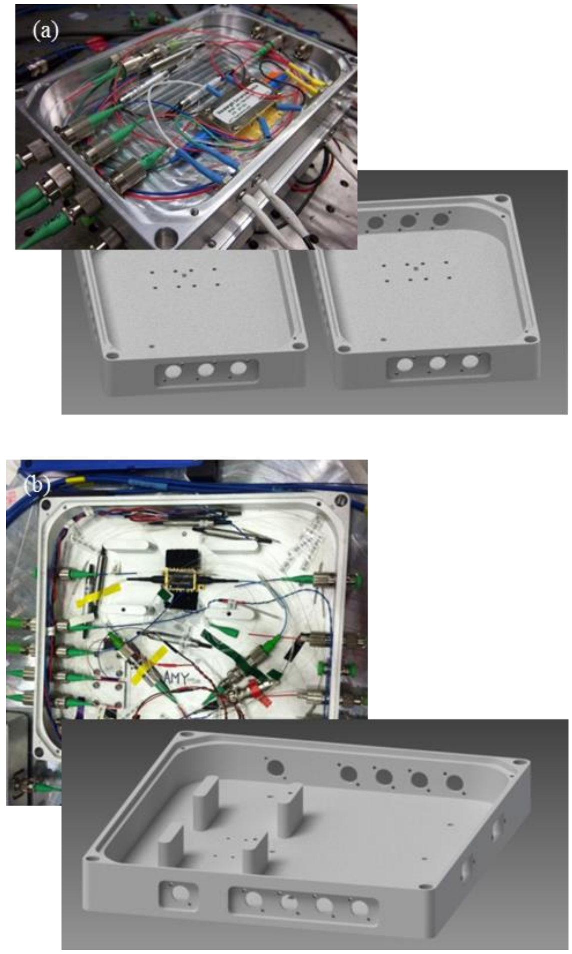

FIG.17: Aluminum housing designs. (a) Two small boxes each measuring 16 cm x 11 cm x 2.5 cm connected by a 22 cm patch cable. (b) Alternate housing consisting of one 18 cm x 20 cm x 2.5 cm box.

The optics package is housed in either two small aluminum boxes of dimensions 16 cm x 11 cm x 2.5 cm (total volume of 0.7 L) connected via a 22 cm patch cable or a single small aluminum box of dimensions 18 cm x 20 cm x 2.5 cm (total volume of 0.9 L), as shown in Fig 17. Once the fiber is placed inside of the boxes, large components are attached to the aluminum housing via room temperature vulcanization (RTV) silicone. Then a two part silicone epoxy is added to the entire volume to provide additional protection from vibrations. The epoxy used for potting is electrically insulating and very soft with a Shore A hardness listed as soft gel. This simple design is similar, although significantly reduced in volume, from the previous 6 L package that was shaken at 0.5 g rms while the comb was fully-stabilized.[49]

APPENDIX E: POWER CONSUMPTION

Table III gives an estimate of the power consumption of the comb system under typical operating conditions inside the laboratory with the exclusion of the power consumption due to the inefficiency of the various power supplies. The total power consumption is driven by three main categories, pump diode laser light generation, temperature control of various sub-systems, and control electronics. Each diode laser is contained within a butterfly package, which has a TEC to control the diode laser temperature.

Table III. Power Consumption of Comb System. The total power consumption can be higher during system start-up than the values given here.

Comb System Element	Typical Current (mA)	Voltage (V)	Typical Power (W)
1480 nm diode laser	700	2.7	2 (x2)
980 nm diode laser	1500	2.7	4 (x2)
Diode laser TEC	500	2.7	1 (x4)
PPLN TEC	--	--	< 1
Femtosecond laser housing TECs	1000	8	8
Commercial photodetectors for f_{opt}, f_{ceo}, and f_{rep}	< 250	15	< 4 (x3)
FPGA-based controller[a]	1800	5	9
Control electronics[b]	200	[c]	5
Total for Comb System	--	--	50

[a] These values do not include the low power consumption high-voltage output.
[b]This includes control electronics for the pump diode laser optical output, the pump diode laser temperature control, the PPLN temperature control, and the femtosecond laser housing temperature control. The actual current to the TECs is listed separately above in the table.
[c]Operating voltages are 5 or 12 V.

REFERENCES

[1] J.L. Hall, Rev. Mod. Phys. **78**, 1279 (2006).
[2] T.W. Hänsch, Rev. Mod. Phys. **78**, 1297 (2006).
[3] S.A. Diddams, J. Opt. Soc. Am. B **27**, B51 (2010).
[4] N.R. Newbury, Nature Photon. **5**, 186 (2011).
[5] A. Schliesser, M. Brehm, F. Keilmann, and D. van der Weide, Opt. Express **13**, 9029 (2005).
[6] I. Coddington, W.C. Swann, and N.R. Newbury, Phys. Rev. Lett. **100**, 013902 (2008).
[7] F. Adler, M.J. Thorpe, K.C. Cossel, and J. Ye, Ann. Rev. Anal. Chem. **3**, 175 (2010).
[8] M. Godbout, J.-D. Deschênes, and J. Genest, Opt. Express **18**, 15981 (2010).
[9] B. Bernhardt, A. Ozawa, P. Jacquet, M. Jacquey, Y. Kobayashi, T. Udem, R. Holzwarth, G. Guelachvili, T.W. Hänsch, and N. Picqué, Nature Photon. **4**, 55 (2010).
[10] E. Baumann, F.R. Giorgetta, W.C. Swann, A.M. Zolot, I. Coddington, and N.R. Newbury, Phys. Rev. A **84**, 062513 (2011).
[11] A.M. Zolot, F.R. Giorgetta, E. Baumann, J.W. Nicholson, W.C. Swann, I. Coddington, and N.R. Newbury, Opt. Lett. **37**, 638 (2012).
[12] J. Roy, J.-D. Deschênes, S. Potvin, and J. Genest, Opt. Express **20**, 21932 (2012).
[13] A.M. Zolot, F.R. Giorgetta, E. Baumann, W.C. Swann, I. Coddington, and N.R. Newbury, J. Quant. Spectrosc. Radiat. Transf. **118**, 26 (2013).
[14] Z. Zhang, T. Gardiner, and D.T. Reid, Opt. Lett. **38**, 3148 (2013).

[15] S. Boudreau, S. Levasseur, C. Perilla, S. Roy, and J. Genest, Opt. Express **21**, 7411 (2013).
[16] G.B. Rieker, F.R. Giorgetta, W.C. Swann, J. Kofler, A.M. Zolot, L.C. Sinclair, E. Baumann, C. Cromer, G. Petron, C. Sweeney, P.P. Tans, I. Coddington, and N.R. Newbury, Optica **1**, 290 (2014).
[17] K. Minoshima and H. Matsumoto, Appl. Opt. **39**, 5512 (2000).
[18] N. Schuhler, Y. Salvade, S. Leveque, R. Dandliker, and R. Holzwarth, Opt. Lett. **31**, 3101 (2006).
[19] P. Balling, P. Kren, P. Masika, and S.A. van den Berg, Opt. Express **17**, 9300 (2009).
[20] I. Coddington, W.C. Swann, L. Nenadovic, and N.R. Newbury, Nature Photon. **3**, 351 (2009).
[21] M. Cui, M.G. Zeitouny, N. Bhattacharya, S.A. van den Berg, H.P. Urbach, and J.J.M. Braat, Opt. Lett. **34**, 1982 (2009).
[22] J. Lee, Y.-J. Kim, K. Lee, S. Lee, and S.-W. Kim, Nature Photon. **4**, 716 (2010).
[23] T.-A. Liu, N.R. Newbury, and I. Coddington, Opt. Express **19**, 18501 (2011).
[24] M.U. Piracha, D. Nguyen, I. Ozdur, and P.J. Delfyett, Opt. Express **19**, 11213 (2011).
[25] E. Baumann, F.R. Giorgetta, I. Coddington, L.C. Sinclair, K. Knabe, W.C. Swann, and N.R. Newbury, Opt. Lett. **38**, 2026 (2013).
[26] X. Wu, H. Wei, H. Zhang, L. Ren, Y. Li, and J. Zhang, Appl. Opt. **52**, 2042 (2013).
[27] E. Baumann, F.R. Giorgetta, J.-D. Deschênes, W.C. Swann, I. Coddington, and N.R. Newbury, Opt. Express **22**, 24914 (2014).
[28] F.R. Giorgetta, W.C. Swann, L.C. Sinclair, E. Baumann, I. Coddington, and N.R. Newbury, Nat. Photon. **7**, 434 (2013).
[29] D.R. Leibrandt, M.J. Thorpe, J.C. Bergquist, and T. Rosenband, Opt. Express **19**, 10278 (2011).
[30] D.R. Leibrandt, J.C. Bergquist, and T. Rosenband, Phys. Rev. A **87**, 023829 (2013).
[31] Q.-F. Chen, A. Nevsky, M. Cardace, S. Schiller, T. Legero, S. Häfner, A. Uhde, and U. Sterr, Rev. Sci. Instrum. **85**, 113107 (2014).
[32] L. Krainer, R. Paschotta, G.J. Spuhler, I. Klimov, C.Y. Teisset, K.J. Weingarten, and U. Keller, Electron. Lett. **38**, 225 (2002).
[33] A. Bartels, D. Heinecke, and S.A. Diddams, Science **326**, 681 (2009).
[34] J. Aus der Au, G.J. Spühler, T. Südmeyer, R. Paschotta, R. Hövel, M. Moser, S. Erhard, M. Karszewski, A. Giesen, and U. Keller, Opt. Lett. **25**, 859 (2000).
[35] C.G. Durfee, T. Storz, J. Garlick, S. Hill, J.A. Squier, M. Kirchner, G. Taft, K. Shea, H. Kapteyn, M. Murnane, and S. Backus, Opt. Express **20**, 13677 (2012).
[36] P. Del'Haye, A. Schliesser, O. Arcizet, T. Wilken, R. Holzwarth, and T.J. Kippenberg, Nature **450**, 1214 (2007).
[37] T.J. Kippenberg, R. Holzwarth, and S.A. Diddams, Science **332**, 555 (2011).
[38] Y. Okawachi, K. Saha, J.S. Levy, Y.H. Wen, M. Lipson, and A.L. Gaeta, Opt. Lett. **36**, 3398 (2011).
[39] F. Tauser, A. Leitenstorfer, and W. Zinth, Opt. Express **11**, 594 (2003).
[40] B. Washburn, R. Fox, N. Newbury, J. Nicholson, K. Feder, P. Westbrook, and C. Jørgensen, Opt. Express **12**, 4999 (2004).
[41] T.R. Schibli, K. Minoshima, F.L. Hong, H. Inaba, A. Onae, H. Matsumoto, I. Hartl, and M.E. Fermann, Opt. Lett. **29**, 2467 (2004).
[42] P. Kubina, P. Adel, F. Adler, G. Grosche, T. Hänsch, R. Holzwarth, A. Leitenstorfer, B. Lipphardt, and H. Schnatz, Opt. Express **13**, 904 (2005).
[43] H. Inaba, Y. Daimon, F.-L. Hong, A. Onae, K. Minoshima, T.R. Schibli, H. Matsumoto, M. Hirano, T. Okuno, M. Onishi, and M. Nakazawa, Opt. Express **14**, 5223 (2006).
[44] N.R. Newbury and W.C. Swann, J. Opt. Soc. Am. B **24**, 1756 (2007).
[45] I. Hartl, G. Imeshev, M.E. Fermann, C. Langrock, and M.M. Fejer, Opt. Express **13**, 6490 (2005).
[46] E. Baumann, F.R. Giorgetta, J.W. Nicholson, W.C. Swann, I. Coddington, and N.R. Newbury, Opt. Lett. **34**, 638 (2009).
[47] J. Lee, K. Lee, Y.-S. Jang, H. Jang, S. Han, S.-H. Lee, K.-I. Kang, C.-W. Lim, Y.-J. Kim, and S.-W. Kim, Sci. Rep. **4**, (2014).
[48] T. Wilken, M. Lezius, T.W. Hansch, A. Kohfeldt, A. Wicht, V. Schkolnik, M. Krutzik, H. Duncker, O. Hellmig, P. Windpassinger, K. Sengstock, A. Peters, and R. Holzwarth, in *CLEO:2013* (Optical Society of America, San Jose, 2013), p. AF2H.5.
[49] L.C. Sinclair, I. Coddington, W.C. Swann, G.B. Rieker, A. Hati, K. Iwakuni, and N.R. Newbury, Opt. Express **22**, 6996 (2014).
[50] S.A. Diddams, T. Udem, J.C. Bergquist, E.A. Curtis, R.E. Drullinger, L. Hollberg, W.M. Itano, W.D. Lee, C.W. Oates, K.R. Vogel, and D.J. Wineland, Science **293**, 825 (2001).
[51] M. Hirano, T. Nakanishi, T. Okuno, and M. Onishi, IEEE J. Sel. Topics Quantum Electron. **15**, 103 (2009).

[52] H. Byun, D. Pudo, J. Chen, E.P. Ippen, and F.X. Kärtner, Opt. Lett. **33**, 2221 (2008).
[53] I. Coddington, W.C. Swann, and N.R. Newbury, Phys. Rev. A **82**, 043817 (2010).
[54] F. Quinlan, T.M. Fortier, M.S. Kirchner, J.A. Taylor, M.J. Thorpe, N. Lemke, A.D. Ludlow, Y. Jiang, and S.A. Diddams, Opt. Lett. **36**, 3260 (2011).
[55] H. Byun, M.Y. Sander, A. Motamedi, H. Shen, G.S. Petrich, L.A. Kolodziejski, E.P. Ippen, and F.X. Kärtner, Appl. Opt. **49**, 5577 (2010).
[56] B.R. Washburn, W.C. Swann, and N.R. Newbury, Opt. Express **13**, 10622 (2005).
[57] R. Paschotta, Opt. Express **18**, 5041 (2010).
[58] C. Kim, K. Jung, K. Kieu, and J. Kim, Opt. Express **20**, 29524 (2012).
[59] J.J. McFerran, W.C. Swann, B.R. Washburn, and N.R. Newbury, Appl. Phys. B **86**, 219 (2007).
[60] S. Wang, C.R. Menyuk, L. Sinclair, I. Coddington, and N.R. Newbury, in *CLEO: 2014* (Optical Society of America, 2014), p. SW3E.4.
[61] K. Tamura and M. Nakazawa, Opt. Lett. **21**, 68 (1996).
[62] N.R. Newbury, B.R. Washburn, K.L. Corwin, and R.S. Windeler, Opt. Lett. **28**, 944 (2002).
[63] K.L. Corwin, N.R. Newbury, J.M. Dudley, S. Coen, S.A. Diddams, B.R. Washburn, K. Weber, and R.S. Windeler, Appl. Phys. B **77**, 269 (2003).
[64] K.L. Corwin, N.R. Newbury, J.M. Dudley, S. Coen, S.A. Diddams, K. Weber, and R.S. Windeler, Phys. Rev. Lett. **90**, 113904 (2003).
[65] J.M. Dudley, G. Genty, and S. Coen, Rev. Mod. Phys. **78**, 1135 (2006).
[66] H.R. Telle, G. Steinmeyer, A.E. Dunlop, J. Stenger, D.H. Sutter, and U. Keller, Appl. Phys. B **69**, 327 (1999).
[67] D.J. Jones, S.A. Diddams, J.K. Ranka, A. Stentz, R.S. Windeler, J.L. Hall, and S.T. Cundiff, Science **288**, 635 (2000).
[68] R. Holzwarth, T. Udem, T.W. Hänsch, J.C. Knight, W.J. Wadsworth, and P.S.J. Russell, Phys. Rev. Lett. **85**, 2264 (2000).
[69] S. Kurimura, Y. Kato, M. Maruyama, Y. Usui, and H. Nakajima, Appl. Phys. Lett. **89**, 191123 (2006).
[70] J.-D. Deschênes, P. Giaccarri, and J. Genest, Opt. Express **18**, 23358 (2010).
[71] H.R. Telle, B. Lipphardt, and J. Stenger, Appl. Phys. B **74**, 1 (2002).
[72] J. Ye, J.L. Hall, and S.A. Diddams, Opt. Lett. **25**, 1675 (2000).
[73] W.C. Swann, J.J. McFerran, I. Coddington, N.R. Newbury, I. Hartl, M.E. Fermann, P.S. Westbrook, J.W. Nicholson, K.S. Feder, C. Langrock, and M.M. Fejer, Opt. Lett. **31**, 3046 (2006).
[74] M.J. Thorpe, D.R. Leibrandt, T.M. Fortier, and T. Rosenband, Opt. Express **18**, 18744 (2010).
[75]The use of trade names is necessary to specify the experimental results and cannot imply endorsement by the National Institute of Standards and Technology.
[76] J.J. McFerran, W.C. Swann, B.R. Washburn, and N.R. Newbury, Opt. Lett. **31**, 1997 (2006).
[77] C.-C. Lee, S. Suzuki, W. Xie, and T.R. Schibli, Opt. Express **20**, 5264 (2012).
[78] Y. Nakajima, H. Inaba, K. Hosaka, K. Minoshima, A. Onae, M. Yasuda, T. Kohno, S. Kawato, T. Kobayashi, T. Katsuyama, and F.-L. Hong, Opt. Express **18**, 1667 (2010).
[79] W.C. Swann, E. Baumann, F.R. Giorgetta, and N.R. Newbury, Opt. Express **19**, 24387 (2011).
[80] J.G. Proakis, *Digital Communications*, 3rd ed. (McGraw-Hill, Boston, Massachusetts, 1995).
[81] C.W. Chou, D.B. Hume, J.C.J. Koelemeij, D.J. Wineland, and T. Rosenband, Phys. Rev. Lett. **104**, 070802 (2010).
[82] N. Hinkley, J.A. Sherman, N.B. Phillips, M. Schioppo, N.D. Lemke, K. Beloy, M. Pizzocaro, C.W. Oates, and A.D. Ludlow, Science **341**, 1215 (2013).
[83] T. Rosenband, D.B. Hume, P.O. Schmidt, C.W. Chou, A. Brusch, L. Lorini, W.H. Oskay, R.E. Drullinger, T.M. Fortier, J.E. Stalnaker, S.A. Diddams, W.C. Swann, N.R. Newbury, W.M. Itano, D.J. Wineland, and J.C. Bergquist, Science **319**, 1808 (2008).
[84] T.R. Schibli, K. Minoshima, F.-L. Hong, H. Inaba, Y. Bitou, A. Onae, and H. Matsumoto, Opt. Lett. **30**, 2323 (2005).
[85] E. Baumann, J.-D. Deschênes, F.R. Giorgetta, W.C. Swann, I. Coddington, and N.R. Newbury, Opt. Lett. **39**, 4776 (2014).
[86] B. Soller, D. Gifford, M. Wolfe, and M. Froggatt, Opt. Express **13**, 666 (2005).